THE JOURNAL OF PHYSICAL CHEMISTRY B

Article

pubs.acs.org/JPCB

Chiroptical Properties of Cryptophane-223 and -233 Investigated by ECD, VCD, and ROA Spectroscopy

Thierry Brotin,*[,†] Nicolas Daugey,[‡] Nicolas Vanthuyne,[§] Erwann Jeanneau,[#] Laurent Ducasse,[‡] and Thierry Buffeteau*[,‡]

[†]Laboratoire de Chimie de l'ENS LYON (UMR 5182-CNRS), École Normale Supérieure de Lyon, 46 Allée d'Italie, 69364 Lyon, France

[‡]Institut des Sciences Moléculaires (UMR 5255-CNRS), Université de Bordeaux, 351 Cours de la Libération, 33405 Talence, France

[§]Aix Marseille Université, Centrale Marseille, CNRS, iSm2 UMR 7313, 13397, Marseille, France

[#]Centre de Diffractométrie Henri Longchambon, Université Lyon 1, 5 rue de La Doua, 69100 Villeurbanne, France

Supporting Information

ABSTRACT: Enantiopure cryptophane derivatives **1** and **2**, possessing linkers of different nature (ethylenedioxy and propylenedioxy) connecting the two cyclotribenzylenes (CTB) units, were separated by HPLC using chiral stationary phases. X-ray crystallographic structures of the four enantiomers (+)-**1**, (−)-**1**, (+)-**2**, and (−)-**2** have been obtained, allowing the unambiguous determination of their absolute configuration (AC) in the solid state. The chiroptical properties of compounds **1** and **2** were determined from polarimetry, electronic circular dichroism (ECD), vibrational circular dichroism (VCD), and Raman optical activity (ROA) experiments and were compared to those of cryptophane-A (**3**) derivative. VCD, ROA and ECD spectra of **1** and **2** were calculated by density functional theory (DFT) and time-dependent density functional theory (TDDFT) calculations, respectively, to confirm the AC of the cryptophane derivatives in solution. The (+)-*PP* and (−)-*MM* configurations were established for compounds **1** and **2** in chloroform solution, as already reported for the two enantiomers of **3**. This result is in agreement with the X-ray structures of the two enantiomers of **1** and **2**.

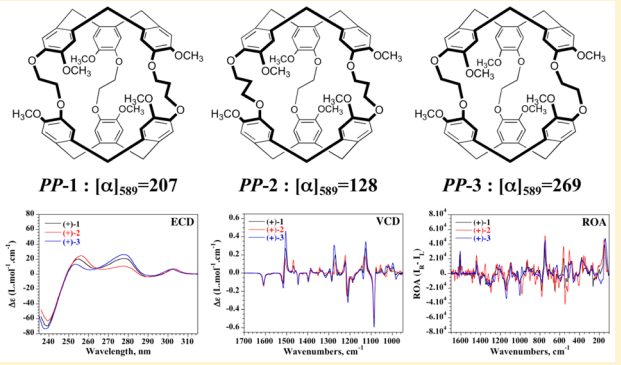

INTRODUCTION

Cryptophane derivatives represent beautiful molecular objects with interesting binding properties toward a large range of guest molecules, such as halogenomethanes and ammonium salts, or atoms in organic or aqueous solutions.[1,2] In the past decade, these molecules have received considerable interest because they complex efficiently monatomic xenon which can be exploited in resonance magnetic imaging in combination with hyperpolarized xenon for the detection of biological targets.[3−12] Consequently, the synthesis of new cryptophanes has been strongly boosted, and chemists have now access to a large range of cryptophane derivatives with different chemical structures and/or symmetries.[13−17]

Besides their interesting binding properties, most of the cryptophane derivatives exhibit an inherently chiral structure. For *anti*-cryptophanes with two identical cyclotribenzylenes (CTB) caps, possessing a D_3-symmetry, the chirality originates from the helical arrangement of the three linkers connecting the two CTB units. The cryptophane-A and its congeners belong to this class of compounds and the two CTB caps possess the same absolute configuration (*MM* or *PP*).[18,19] *syn*-Cryptophanes with two different CTB caps, possessing a C_3-symmetry, are also chiral molecules but the chirality comes from the fact that the two CTB units possess opposite absolute configuration (*MP* or *PM*). The cryptophane-D and the recently prepared nonamethoxy cryptophane belong to this class of compounds.[20,21]

During the past decade, several enantiopure cryptophane-A derivatives have been thoroughly studied by chiroptical techniques such as polarimetry, electronic circular dichroism (ECD), and vibrational circular dichroism (VCD) and, more recently, by Raman optical activity (ROA).[13,21−36] We have demonstrated that these compounds exhibit very different chiroptical properties depending on their symmetry and the nature of the substituents attached on the benzene rings. In addition, we have observed that the chiroptical properties of some water-soluble cryptophanes are strongly modified by external parameters such as the nature of the solution (LiOH/H_2O, NaOH/H_2O, KOH/H_2O, or CsOH/H_2O) and the nature of the guest species inside the cavity.[27−32,34] For

Received: May 12, 2015
Revised: June 19, 2015
Published: June 19, 2015

DOI: 10.1021/acs.jpcb.5b04539
J. Phys. Chem. B 2015, 119, 8631−8639

instance, important modifications of the chiroptical properties of water-soluble cryptophanes have been observed in basic conditions upon encapsulation of cationic species (cesium or thallium cations).[31,32,34] However, except for enantiopure cryptophanes E and G studied Collet and co-workers,[22] the chiroptical properties of cryptophanes concern only cryptophane-A derivatives possessing three ethylenedioxy linkers connecting the two CTB units. Thus, there is an interest to study the chiroptical properties of cryptophane derivatives possessing different chemical structures or symmetry.

The cryptophane-223 and -233 (compounds **1** and **2** in Scheme 1), whose the synthesis of racemates have been reported in 2003,[37] differ from cryptophane-A (compound **3** in Scheme 1) because of the presence of an additional methylene group into one or two linkers, respectively. In addition, these two molecules possess a C_2-symmetry whereas cryptophane-A possesses a D_3-symmetry. Cryptophane-223 (**1**) possesses two ethylenedioxy bridges (in blue, Scheme 1) and a single propylenedioxy bridge (in red, Scheme 1), whereas cryptophane-233 (**2**) possesses two propylenedioxy bridges and a single ethylenedioxy bridge. Thus, compounds **1** and **2** are expected to have a larger inner cavity and to be more flexible than compound **3**. These structural modifications may certainly induce larger chiroptical changes upon encapsulation of guest species than those observed for the more rigid cryptophane-A skeleton.

Scheme 1. Chemical Structure of Cryptophane-223 (1), Cryptophane-233 (2), and Cryptophane-A(3)

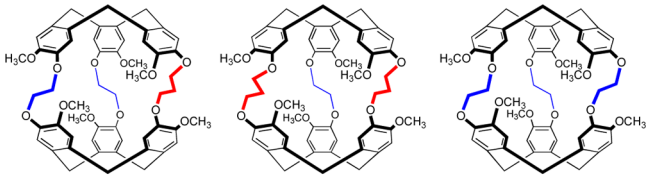

cryptophane-223 (1) cryptophane-233 (2) cryptophane-A (3)

In this article, we investigate in detail the chiroptical properties of enantiopure cryptophane-223 (**1**) and -233 (**2**) in solution. The efficient separation of the two enantiomers of molecules **1** and **2** by high performance liquid chromatography (HPLC) has given us the opportunity to investigate the chiroptical properties of these hosts by polarimetry, ECD, VCD, and ROA. The absolute configuration (AC) of molecules **1** and **2** has been determined in solution from ECD, VCD and ROA experiments associated with theoretical calculations using density functional theory (TDDFT for ECD and DFT for VCD and ROA). These AC have been compared with those obtained in the solid state from the X-ray crystallographic structures of the four enantiomers (+)-**1**, (−)-**1**, (+)-**2**, and (−)-**2**. Finally, the spectroscopic results have been compared to those obtained for cryptophane-A in order to establish a relationship between the chemical structure of these derivatives and their chiroptical properties.

EXPERIMENTAL SECTION

Synthesis of Cryptophanes 1−2. The racemic mixture of cryptophanes **1** and **2** were prepared according to a known procedure.[37] Enantiopure cryptophanes **1−2** have been obtained as described below.

Chiral Separation of 1 and 2 by HPLC. The chiral separation of compounds **1** and **2** was conducted on a semipreparative Chiralpak IA column (250 × 10 mm), thermostated at 30 °C using hexane/EtOH/$CHCl_3$ (20/40/40) as mobile phase. The flow rate was 5 mL/min. UV−vis detection was performed at 254 nm. 250 injections (1 mL) every 14 min were necessary to separate the two enantiomers of the racemic mixture of **1** (405 mg). Similarly, 200 injections (500 μL) every 13 min were necessary to separate the two enantiomers of the racemic mixture of **2** (150 mg).

X-ray Crystallography. Suitable crystals of enantiomers (+)-**1**, (−)-**1**, (+)-**2**, and (−)-**2** were selected and mounted on a Gemini κ-geometry diffractometer equipped with an Atlas CCD detector and using Cu radiation (λ = 1.5416 Å). Intensities were collected at 150 K using the CrysalisPro software.[38] Reflection indexing, unit-cell parameters refinement, Lorentz-polarization correction, peak integration and background determination were carried out with the CrysalisPro software.[38] An analytical absorption correction was applied using the modeled faces of the crystal.[39] The resulting set of *hkl* was used for structure solution and refinement. The structures were solved by direct methods with SIR97,[40] and the least-squares refinement on F^2 was achieved with the CRYSTALS software.[41] All non-hydrogen atoms were refined anisotropically. The hydrogen atoms were all located in a difference map, but those attached to carbon atoms were repositioned geometrically. The H atoms were initially refined with soft restraints on the bond lengths and angles to regularize their geometry (C−H in the range 0.93−0.98 Å and U_{iso}(H) in the range 1.2−1.5 times U_{eq} of the parent atom), after which the positions were refined with riding constraints. For compound (+)-**1** and (−)-**1**, two chloroform molecules could be located inside and outside the cryptophane cage. Nevertheless, these structures contain additional solvent molecules outside the cryptohane cages that could not be localized. Structures (+)-**2** and (−)-**2** had remaining electron density within the cryptophane cage but the solvent molecules could not be modeled. In all four structures the contribution of the disordered solvent molecules was removed using the SQUEEZE algorithm.[42]

CCDC 1045695, 1045696, 1045697, and 1045698 contain the crystallographic data of (+)-**1**, (−)-**2**, (+)-**2**, and (−)-**1**, respectively. These data can be obtained free of charge from The Cambridge Crystallographic Data Centre via www.ccdc.cam.ac.uk/data_request/cif.

Polarimetric, UV−vis and ECD Measurements. Optical rotations of compounds (+)-**1**, (−)-**1**, (+)-**2**, and (−)-**2** were measured in $CHCl_3$ at several wavelengths using a polarimeter with a 100 mm cell thermostated at 25 °C. UV−vis and ECD spectra were recorded in two solvents ($CHCl_3$, CH_2Cl_2) at 20 °C with a 0.2 cm (or 1 cm) path length quartz cell. The concentration of compounds **1−2** was taken in the range 5×10^{-5}−1.1×10^{-4} M. Spectra were recorded in the 220−400 nm wavelength range with a 0.5 nm increment and a 1 s integration time. Spectra were processed with standard spectrometer software, baseline corrected and slightly smoothed by using a third order least-squares polynomial fit. Spectral units were expressed in difference of molar extinction coefficients.

IR and VCD Measurements. The infrared and VCD spectra were recorded with a FTIR spectrometer equipped with a VCD optical bench.[43] IR absorption and VCD spectra were recorded at a resolution of 4 cm^{-1}, by coadding 50 scans and 24000 scans (8 h acquisition time), respectively. Samples were held in a variable path length cell with BaF_2 windows. IR and VCD spectra of the two enantiomers of compounds **1−2** were measured in $CDCl_3$ solvent at a concentration of 0.015 M and

DOI: 10.1021/acs.jpcb.5b04539
J. Phys. Chem. B 2015, 119, 8631−8639

at a path length of 250 μm. In all experiments, the photoelastic modulator was adjusted for a maximum efficiency at 1400 cm^{-1}. Calculations were done with the standard spectrometer software, using Happ and Genzel apodization, de-Haseth phase-correction and a zero-filling factor of 1. Calibration spectra were recorded using a birefringent plate (CdSe) and a second BaF_2 wire grid polarizer, following the experimental procedure previously published.[44] Finally, in the presented IR spectra, the solvent absorption was subtracted out.

Raman and ROA Measurements. Raman and ROA spectra were recorded at ambient temperature on a ChiralRAMAN spectrometer (BioTools, Inc.), equipped with a Millennia PRO 2sJ (Spectra-Physics) diode-pumped solid-state laser (Nd:YV04) operating at 532 nm. This spectrometer employs backscattering geometry and scattered circular polarization (SCP) setup as designed by W. Hug.[45,46] The ROA spectra are presented as intensity differences ($I_R - I_L$), with I_R and I_L denoting the Raman scattered intensities with right- and left-circular polarization states, respectively. The two enantiomers of cryptophanes **1**−**2** were dissolved in $CDCl_3$ to a concentration of 0.1 M and filled into ROA fused silica microcell (4 × 3 × 10 mm, BioTools, Inc.). The power of the laser was 200 mW (~80 mW at the sample). Each presented spectrum is an average over about 20 h of spectra of 15 min acquisition time, corresponding to 1376 scans. The exposure time was 0.367 s to prevent saturation of the CCD detector. Raman and ROA spectra were collected in the range 2500−100 cm^{-1} with spectral resolution of about 7 cm^{-1}. All measured spectra were exported into the Origin 7.5 software package for data treatment and figure preparation. After removing the artifact spikes (false CCD detector signal, coming from cosmic rays), the ROA spectra were averaged and slightly smoothed (Stavisky−Golay algorithm, 9 points). A ROA spectrum of the solvent, recorded with the same experimental conditions, was subtracted from the bare ROA spectra of the samples to remove the artifact signal of the solvent.

DFT and TDDFT Calculations. The geometry optimizations, vibrational frequencies and absorption intensities were calculated by the Gaussian 09 program[47] on the DELL cluster of the MCIA computing center of the University Bordeaux. Calculations of the optimized geometry of $CHCl_3$@*PP*-**1** and $CHCl_3$@*PP*-**2** complexes were performed at the density functional theory (DFT) level using B3PW91 functional[48] and 6-31G** basis set.[49] The geometries of the complexes were optimized from their crystal structures as a starting point. Structures with respectively *trans* (*T*) and *gauche*−*gauche* (*GG*) conformations for the ethylenedioxy and propylenedioxy linkers were optimized, which are quite close to the X-ray structure. Vibrational frequencies and IR intensities were calculated at the same level of theory. For comparison to experiment, the calculated frequencies were scaled by 0.968 and the calculated intensities were converted to Lorentzian bands with a half-width of 7 cm^{-1}.

The UV−vis (excitation energies and associated oscillator strengths) and ECD spectra (excitation energies and rotational strengths) were calculated by time-dependent density functional theory (TDDFT) using the MPW1K functional containing 42.8% of HF exchange[50] and the 6-31+G* basis set. The calculations were performed using the Gaussian 09 package,[47] taking into account the solvent (chloroform) effects within the integral equation formalism of the polarizable continuum model (IEFPCM).[51,52] Other functionals/basis sets were used but the MPW1*K*/6-31+G* approach was found to give reliable results against the overall shape of the UV−vis and ECD spectra. In particular, the ECD spectra calculated using a small basis, such as the 6-31G* basis set, does not compare well with experiment thus showing that it is quite important to introduce diffuse functions. For comparison to experiment, each transition of UV−vis (or ECD) spectrum has been enlarged using a Gaussian function having a full width at half-maximum (fwhm) of 0.1 and 0.05 eV for UV−vis and ECD, respectively.

RESULTS AND DISCUSSION

Separation of Enantiomers of Compounds 1 and 2 by HPLC. Preparative HPLC on chiral stationary phase has been used to separate the two enantiomers of cryptophane-223 (**1**) and cryptophane-233 (**2**). Chiralpak IA column provided the best conditions to separate the two enantiomers of compounds **1** and **2** using a mixture of solvents (hexane/EtOH/$CHCl_3$, 20/40/40). A very good separation was obtained in these conditions for both compounds (see Figure 1). For compound

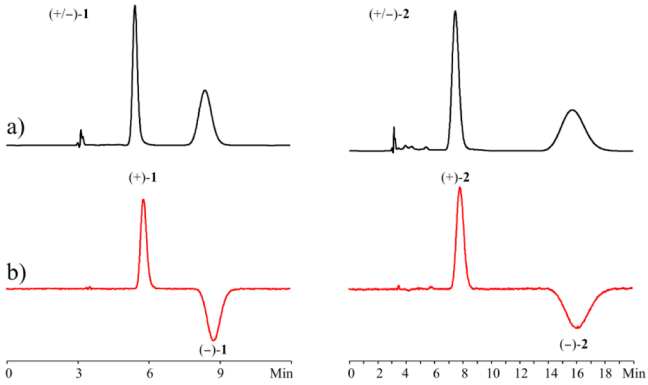

Figure 1. Separation of the two enantiomers of **1** and **2** by using analytical chiral HPLC column (Chiralpak IA, hexane/EtOH/$CHCl_3$ (20/40/40), 1 mL/min). (a) Detection by UV−vis (254 nm). (b) Detection by CD at 254 nm.

1, the enantiomer (+)-**1** was first eluted (t_1 = 5.45 min) followed by the enantiomer (−)-**1** (t_2 = 8.4 min, α = 2.21). In the case of compound **2**, in the same eluting conditions, the enantioselectivity is better (α = 2.84), the first eluted enantiomer was (+)-**2** (t_1 = 7.5 min and t_2 = 15.7 min). Detection of the two enantiomers was achieved with UV−vis detector connected to a circular dichroism detector, giving the CD sign at 254 nm for each enantiomer in the eluent used for chromatography (Figure 1, part a and b as well as Supporting Information, Figures S1−S2). It is noteworthy that despite these favorable separation conditions, a small quantity of each enantiomer was obtained due to the very low solubility of the two molecules. Indeed, for both compounds, several liters of mobile phase were necessary to get the desired enantiomers in fair quantities. Thus, from 405 mg of racemic compound **1**, 185 mg of (+)-**1** (ee >99.5%) and 185 mg of (−)-**1** (ee >99.5%) were isolated. Similarly, from 150 mg of racemic compound **2**, 70 mg of (+)-**2** (ee >98.5%) and 70 mg of (−)-**2** (ee >99.3%) were isolated.

After evaporation of mobile phase, an additional purification step, consisting of a chromatography on silica gel (CH_2Cl_2/acetone, 90/10) followed by a crystallization in a $CHCl_3$/EtOH mixture, has been applied to the two enantiomers of compounds **1** and **2**. This procedure ensures a good chemical

DOI: 10.1021/acs.jpcb.5b04539
J. Phys. Chem. B 2015, 119, 8631−8639

Table 1. Crystallographic Data of Enantiomers (+)-1, (−)-1, (+)-2, and (−)-2

enantiomers	(+)-1	(−)-1	(+)-2	(−)-2
chemical formula	$C_{55}H_{56}O_{12}\cdot 2(CHCl_3)$	$C_{55}H_{56}O_{12}\cdot 2(CHCl_3)$	$C_{56}H_{58}O_{12}$	$C_{56}H_{58}O_{12}$
molecular weight	1147.73 g·mol^{-1}	1147.73 g·mol^{-1}	923.07 g·mol^{-1}	923.07 g·mol^{-1}
crystal system	monoclinic	monoclinic	trigonal	trigonal
space group	$P2_1$	$P2_1$	$P3_1$	$P3_2$
Z	2	2	3	3
unit-cell parameters	a = 12.8647(6) Å	a = 12.8675(8) Å	a = 12.1667(6) Å	a = 12.1534(4) Å
	b = 11.9718(5) Å	b = 11.9406(6) Å	b = 12.1667(6) Å	b = 12.1534(4) Å
	c = 20.6433(9) Å	c = 20.642(1) Å	c = 30.158(2) Å	c = 30.058(1) Å
	α = 90°	α = 90°	α = 90°	α = 90°
	β = 106.783(5)°	β = 106.804(6)°	β = 90°	β = 90°
	γ = 90°	γ = 90°	γ = 120°	γ = 120°
volume	3043.9 (2) Å^3	3036.1 (3) Å^3	3866.2(4) Å^3	3844.9(4) Å^3
$R[F^2 > 2\sigma(F^2)]$	0.096	0.112	0.047	0.037
$wR(F^2)$	0.243	0.174	0.131	0.105
GoF	0.98	1.02	0.95	0.97
no. of reflections ($I > 2.0\sigma(I)$)	9368	8909	7483	9077
no. parameters	713	686	614	615
no. of restraints	9	37	1	1
residual density	−0.76 e Å^{-3}	−0.79 e Å^{-3}	−0.22 e Å^{-3}	−0.16 e Å^{-3}
	1.03 e Å^{-3}	0.75 e Å^{-3}	0.20 e Å^{-3}	0.19 e Å^{-3}
Flack parameter	0.09(3)	0.06(3)	−0.013(5)	−0.009(2)

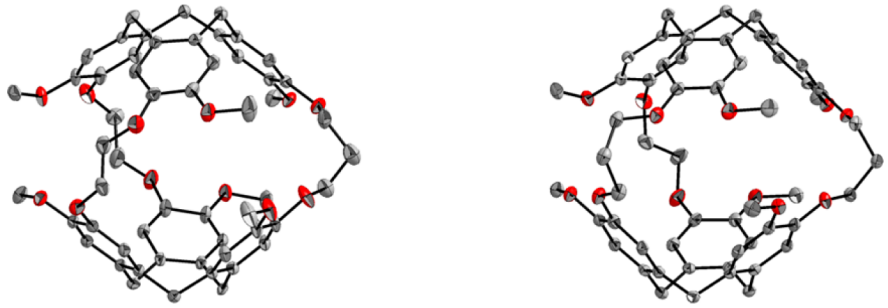

Figure 2. X-ray structures of compounds *PP*-**1** and *PP*-**2**.

purity of the compounds **1** and **2** as well as an excellent enantiomeric excess for each enantiomer.

X-ray Crystallographic Structures. Good quality single-crystals have been obtained for the two enantiomers of **1** and **2** by slow evaporation of $CHCl_3$/EtOH mixtures. The X-ray structures, reported in Table 1, reveal that the unit cells are different for the two compounds **1** and **2**. The two enantiomers of **1** crystallize in a monoclinic $P2_1$ space group with two molecules per unit cell (Supporting Information, Figure S3) whereas the two enantiomers of **2** crystallize in a trigonal $P3_1$ and $P3_2$ space groups with three molecules per unit cell (Supporting Information, Figure S4). In addition, the unit cells of (+)-**1** and (−)-**1** exhibit large intermolecular volumes suitable for accommodating solvent molecules, whereas the unit cells of (+)-**2** and (−)-**2** show smaller interstitial voids. For instance, enantiomers (+)-**1** and (−)-**1** display intermolecular voids of about 207 and 233 Å^3 per cryptophane molecule, respectively. These volumes represent approximately 15% of the total unit cell volume and the SQUEEZE analysis performed on the X-ray diffraction data gives an estimate of nearly 500 e-/unit-cell. This corresponds to four additional chloroform molecules per unit cell. For enantiomers (+)-**2** and (−)-**2**, the interstitial voids were found too small (lower than 70 Å^3 per unit cell) to accommodate solvent molecules. While the chloroform molecule lying in the cavity of the cryptophanes could be modeled for **1**, the strong disorder present in **2** prevented the $CHCl_3$@cryptophane complexes to be modeled.

The X-ray structures of cryptophanes **1** and **2** are shown in Figure 2 for the $CHCl_3$@(+)-**1** and $CHCl_3$@(+)-**2** complexes (the chloroform molecules have been removed for clarity). A closer examination of these structures shows that the ethylenedioxy and propylenedioxy bridges possess *trans* and *gauche* conformations, respectively. For instance, the X-ray structure of compound (+)-**1** shows that the propylenedioxy linker possesses a *gauche*−*gauche* conformation whereas the two ethylenedioxy linkers possess a *trans* conformation. This situation is also observed for the enantiomer (−)-**1**. The X-ray structure of compounds (+)-**2** and (−)-**2** reveals that the two propylenedioxy bridges have a preferential *gauche*−*gauche* conformation, whereas the ethylenedioxy linker possess a *trans* conformation. It is noteworthy that the *gauche*−*gauche* conformation of the propylenedioxy bridges observed for **1** and **2** reduces significantly the cavity size of these cryptophanes, as revealed by the intramolecular volumes determined for the different structures (Table 2). The values of these intramolecular volumes (96.5 and 98.2 Å^3 for **1** and **2**, respectively) are similar to that determined for cryptophane-A (**3**) with an all *trans* conformation of the ethylenedioxy linkers (ca. 95 Å^3). As already mentioned for cryptophane-A molecule, this range of

DOI: 10.1021/acs.jpcb.5b04539
J. Phys. Chem. B 2015, 119, 8631−8639

Table 2. Inter- and Intramolecular Volumes Calculated from X-ray Crystallographic Structures

enantiomers	intermolecular volume, Å^3	intramolecular volume, Å^3
(+)-**1**	207	100
(−)-**1**	233	93
(+)-**2**	21	98
(−)-**2**	24	99

cavity size matches very well with the chloroform (ca. 72 Å^3), allowing its encapsulation.

The refinement of the Flack parameter allowed the determination of the absolute configuration of enantiomers (+)-**1**, (−)-**1**, (+)-**2** and (−)-**2**. From the X-ray structures of the four compounds, we can assign with confidence the *PP* absolute configuration for the enantiomers (+)-**1** and (+)-**2**. Similarly, the *MM* absolute configuration can be assigned to the enantiomers (−)-**1** and (−)-**2**. These results are in agreement with the absolute configuration previously determined for the two enantiomers of cryptophane-A ((+)-*PP*-**3** and (−)-*MM*-**3**).[20]

Polarimetry and ECD Spectroscopy. Optical rotation values for both enantiomers of compounds **1** and **2** have been measured in $CHCl_3$ solutions at several wavelengths (Table 3). These optical rotation values have been compared with those measured for the two enantiomers of cryptophane-A, (+)-**3** and (−)-**3**, under the same experimental conditions.[24] Even though the chemical structure of the three cryptophanes is similar, a significant difference in the magnitude of the optical rotation values was observed. Thus, at 589 nm (+)-**3** have the highest optical rotation value ($[\alpha]^{25}_{589} = +269 \times 10^{-1}$ deg cm^2 g^{-1}). The $[\alpha]^{25}_{589}$ value decreases to $+207 \times 10^{-1}$ deg cm^2 g^{-1} for compound (+)-**1** and $+128.2 \times 10^{-1}$ deg cm^2 g^{-1} for compound (+)-**2**. These results reveal the correlation between the flexibility (i.e., presence of *gauche* conformations) of the linkers and the magnitude of the optical rotation values measured at a given wavelength. Indeed, in a previous work, we have shown that the presence of *gauche* conformations for **3** decreased the optical rotation values.[26] For experiments in $CHCl_3$ solution, optical rotation value of $[\alpha]^{25}_{589} = -274 \times 10^{-1}$ deg cm^2 g^{-1} was measured for the $CHCl_3$@(−)-**3** complex, possessing a preferential all-*trans* conformation of the linkers. The $[\alpha]^{25}_{589}$ value decreased to -234 and -207×10^{-1} deg cm^2 g^{-1} for measurements in CH_2Cl_2 (a molecule having a smaller size with respect to chloroform) and $C_2H_2Cl_4$ (a molecule which can not enter the cavity of **3**), respectively. The decrease of the optical rotation values was interpreted by the presence of *gauche* conformations in the linkers for cryptophanes binding guest molecules with small size (the presence of *gauche* conformations decreases the size of the cavity to stabilize the CH_2Cl_2@(−)-**3** complex) and for empty cryptophane. For cryptophane-223 and -233, the propylenedioxy linkers may adopt higher conformation possibilities (ca. 9) than ethylenedioxy linkers (ca. 3).[53] In addition, the probability to have at least one *gauche* conformation is higher for propylenedioxy linkers than for ethylenedioxy linkers. Consequently, compound **2**, which possesses two propylenedioxy linkers, shows the lowest optical rotation values.

UV−vis and ECD spectra for both enantiomers of **1** and **2** have been measured in $CHCl_3$ solutions. The UV−vis spectra of **1** and **2** reveal two broad bands in the 235−320 nm spectral range (Supporting Information, Figure S5). These two bands correspond to the two forbidden ^1L_a and ^1L_b transitions (Platt's notation) of the phenyl rings. The band of moderate intensity (15000−15700 L.mol^{-1}.cm^{-1}) located in the 265−315 nm region corresponds to the ^1L_b transition of the phenyl rings. The second band located at lower wavelength (235−265 nm), possessing a larger intensity (37500−39500 L·mol^{-1}·cm^{-1}), corresponds to the ^1L_a transition. It is noteworthy that the ^1L_b transition is slightly affected by the presence of propylenedioxy linkers. Indeed, a shoulder appears at 300 nm, which increases in intensity with the number of propylenedioxy linkers.

ECD spectra recorded in the 235−320 nm spectral range for both enantiomers of **1** and **2** are reported in Supporting Information (Figure S6, parts a and b, respectively), whereas the comparison of experimental ECD spectra of (+)-**1**, (+)-**2**, and (+)-**3** are presented in Figure 3. As shown in Figure 3, the

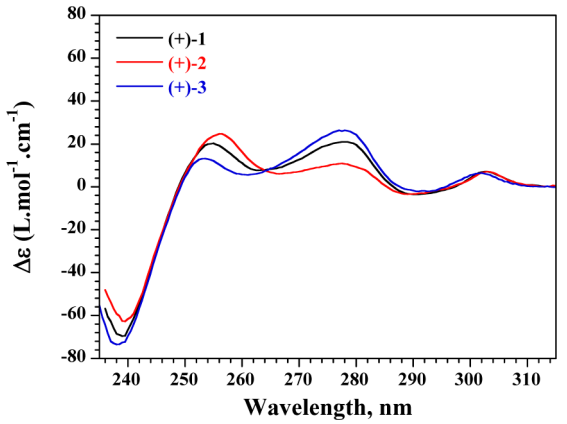

Figure 3. Comparison of experimental ECD spectra of (+)-**1** (black spectrum), (+)-**2** (red spectrum), and (+)-**3** (blue spectrum) in $CHCl_3$ solution.

ECD spectra of (+)-**1** and (+)-**2** are similar to the one published for (+)-**3**.[13,21] The only spectral difference concerns the 250−285 nm region, where the ECD component at 255 nm

Table 3. Optical Rotation (10^{-1} deg cm^2 g^{-1}) of the Two Enantiomers of Compounds 1−3, Recorded at 298 K at Several Wavelengths in $CHCl_3$

compd	solvent	concn[b]	$[\alpha]^{25}_{589}$	$[\alpha]^{25}_{577}$	$[\alpha]^{25}_{546}$	$[\alpha]^{25}_{436}$	$[\alpha]^{25}_{365}$
(+)-**1**	$CHCl_3$	0.27	+ 207.0	+217.9	+251.9	+468.7	+878.3
(−)-**1**	$CHCl_3$	0.28	−209.1	−220.1	−254.7	−468.6	−877.3
(+)-**2**	$CHCl_3$	0.28	+128.2	+134.3	+156.3	+290.5	+547.7
(−)-**2**	$CHCl_3$	0.27	−128.3	−134.0	−154.8	−285.4	−533.0
(+)-**3**[a]	$CHCl_3$	0.17	+269.0	+284.0	+326.5	+626.5	+1152.0
(−)-**3**[a]	$CHCl_3$	0.13	−274.0	−288.0	−332.0	−623.0	−1154.0

[a]For comparison, optical rotations of the two enantiomers of cryptophane-A are reported in the same solvent. [b]g/100 mL.

DOI: 10.1021/acs.jpcb.5b04539
J. Phys. Chem. B 2015, 119, 8631−8639

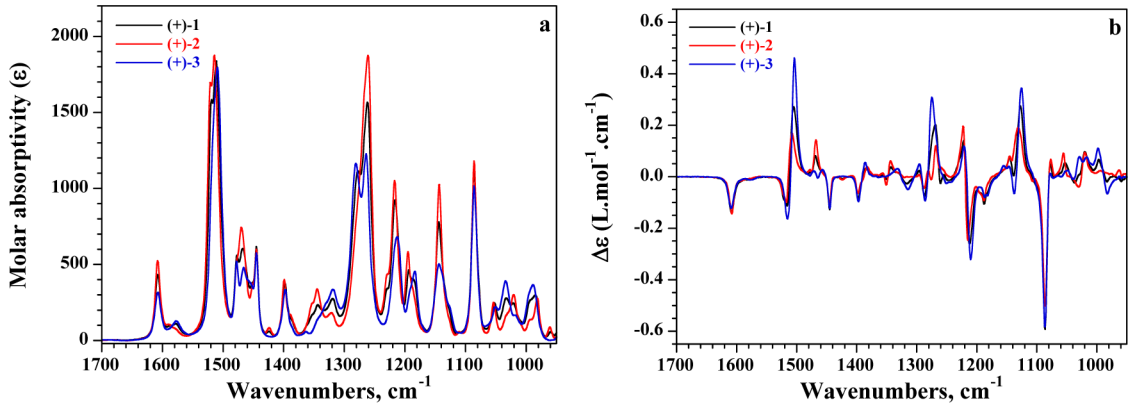

Figure 4. Comparison of experimental (a) IR and (b) VCD spectra of (+)-**1** (black spectrum), (+)-**2** (red spectrum), and (+)-**3** (blue spectrum) in $CDCl_3$ solution (15 mM, 250 μm path length).

increases with the number of propylenedioxy linkers, whereas the component at 278 nm decreases. In contrast, the ECD spectra in the ^1L_b region are not perturbed by the change of the chemical structure of the three linkers. As previously mentioned in the literature, the ^1L_b region is very sensitive to the solvent, the nature of the guest, and the substitution of the CTB units.[13,21,27] Since the CTB units of the compounds **1**-**3** are identical, only very small spectral modifications are expected in the ^1L_b region for ECD spectra recorded under the same experimental conditions, as observed in Figure 3. On the other hand, the bisignate pattern observed in the ^1L_a region has been previously used to determine the absolute configuration (AC) of **3** or hemicryptophane derivatives.[54] It has been found that the *PP* (respectively, *MM*) configuration displays in the ^1L_a region a couplet structure with a negative−positive (respectively, positive−negative) sequence from short to long wavelength. By analogy with these results, the *PP* configuration can be assigned to the (+)-**1** and (+)-**2** compounds. In turn, the *MM* configuration can be assigned to the (−)-**1** and (−)-**2** compounds. To confirm these results and determine unambiguously the absolute configuration of these two cryptophane derivatives, we have performed TDDFT calculations to predict the ECD spectra of *PP*-**1** and *PP*-**2** compounds. The comparison of the experimental ECD spectra of (+)-**1** and (+)-**2** recorded in $CHCl_3$ solutions with the predicted ECD spectra for the *PP* configuration are presented in Supporting Information (Figures S7 and S8). The TDDFT calculations have been performed assuming a *trans* (*T*) and the *gauche*−*gauche* (*GG*) conformations for the ethylenedioxy and propylenedioxy linkers, respectively. Despite the fact that TDDFT calculations have been performed for an unique conformation of the linkers, the overall shape of the predicted ECD spectra reproduces fairly well the experimental ECD spectra of compound (+)-**1** and (+)-**2**. For example, the negative−positive couplets observed on the experimental spectra for the ^1L_a transition of (+)-**1** and (+)-**2** (Figure 3), is perfectly reproduced on the spectra calculated for the *PP* configuration of **1** and **2**, confirming the *PP* configuration of these cryptophane derivatives. This result corroborates the AC determined by X-ray crystallography.

IR and VCD Spectroscopy. The chiroptical properties of enantiopure cryptophanes **1**−**2** have been also investigated by vibrational circular dichroism (VCD). IR and VCD experiments of the two enantiomers of compounds **1**−**2** have been performed in $CDCl_3$ solutions (0.015 M). The IR spectra of **1** and **2** are reported in Supporting Information (Figure S9a) in the 1700−950 cm^{-1} spectral range, whereas the comparison (+)-**1**, (+)-**2**, and (+)-**3** are presented in Figure 4a. Most of the bands observed in the IR spectra of **1**−**2** have been assigned for other cryptophane-A derivatives.[25,26] Comparison of the IR spectra of **1** and **2** reveals several spectral differences (Supporting Information, Figure S9a). The spectral modifications observed on the IR spectrum of compound **2** concern in particular a slight shift at higher wavenumbers of the 1510 cm^{-1} band associated with the $\nu_{19b}C{=}C$ stretching vibration of the phenyl rings, an increase of the intensity of the 1469 cm^{-1} band associated with the δCH_2 bending vibration, the inversion of the relative intensity of the two bands located at 1344 and 1318 cm^{-1} ascribed to the wagging of the CH_2 groups of the ethylenedioxy and propylenedioxy linkers, respectively, and the decrease of the bands at 1033 and 993 cm^{-1} assigned to the $\nu_s C{-}O{-}C$ stretching of dioxy linkers coupled to $\nu C{-}C$ and ring modes, respectively. All of these modifications are perfectly reproduced by the DFT calculations (Supporting Information, Figure S9b), allowing the discrimination between the two compounds by using IR spectroscopy.

The VCD spectra of the two enantiomers of compounds **1** and **2** are reported in Supporting Information (Figures S10a and S10b, respectively) in the 1700−950 cm^{-1} spectral range, whereas the comparison of experimental VCD spectra of (+)-**1**, (+)-**2**, and (+)-**3** are presented in Figure 4b. As shown in Figure S10a and S10b, the overall shape of the VCD spectra is similar for cryptophane-223 and −233. The signs of the different bands of (+)-enantiomers (or (−)-enantiomers) are not modified by the nature (ethylenedioxy or propylenedioxy) of the linkers. Nevertheless, as shown in Figure 4b, several modifications in the band's intensity are observed for the two compounds. Thus, the intensity of bands at 1506, 1270, 1126, and 1086 cm^{-1} slightly decreases on the VCD spectra of compound **2**. In addition, the bands observed at 1316 and 996 cm^{-1} on the VCD spectra of **1** disappear on the VCD spectra of **2**. In contrast, the intensity of the bands at 1468 and 1344 cm^{-1} increases on the VCD spectra of **2**. Moreover, the comparison of the VCD spectra of **1** and **2** with the one of **3**, reveals that the VCD spectrum of **1** is approximately the half-sum of the VCD spectra of **2** and **3**. This feature suggests that the conformations of ethylenedioxy (ca. *trans*) and propylenedioxy (ca. *gauche*−*gauche*) linkers seem not to be modified for the three compounds. Thus, the intensities of the bands at 1506, 1270, and 1126 cm^{-1} are directly related to the conformational

DOI: 10.1021/acs.jpcb.5b04539
J. Phys. Chem. B 2015, 119, 8631−8639

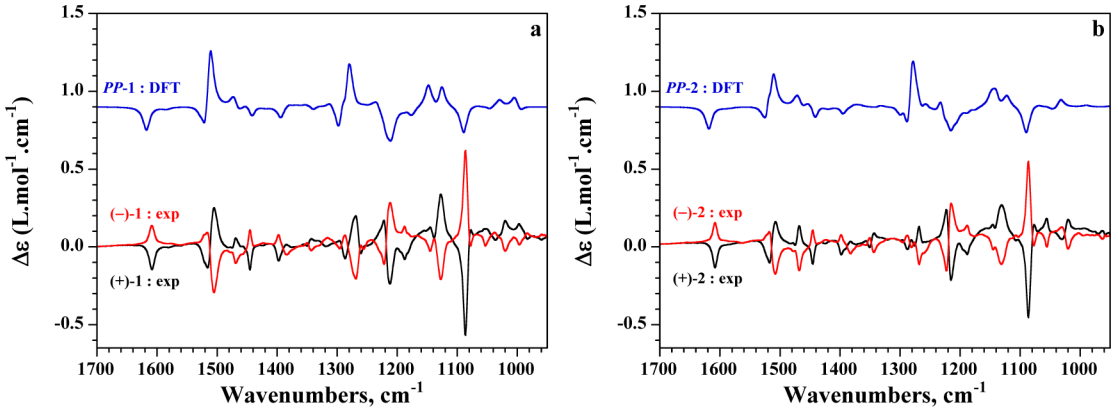

Figure 5. Comparison of experimental VCD spectra of a) (+)-**1** (black spectrum) and (−)-**1** (red spectrum) and b) (+)-**2** (black spectrum) and (−)-**2** (red spectrum) in $CDCl_3$ solution (15 mM, 250 μm path length) and calculated VCD spectra of (a) $CHCl_3$@*PP*-**1** and (b) $CHCl_3$@*PP*-**2** complexes at the B3PW91/6-31G** level for the *trans* and *gauche*−*gauche* conformations of the ethylenedioxy and propylenedioxy linkers, respectively.

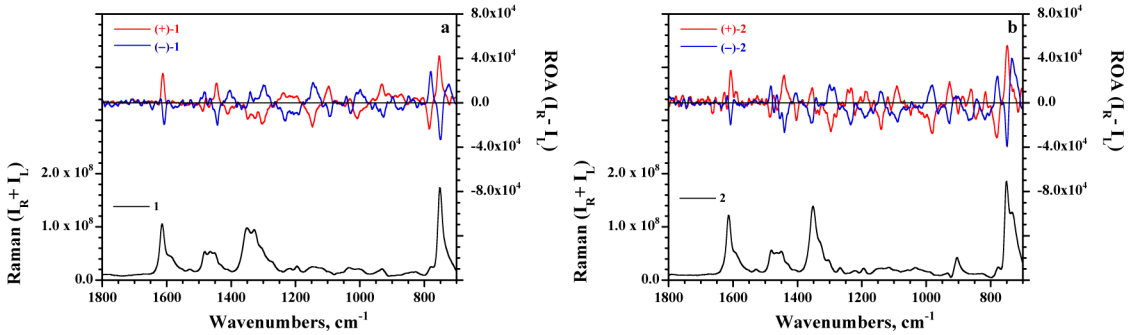

Figure 6. (a) Solvent-corrected Raman and ROA spectra recorded at 295 K of (+)-**1** and (−)-**1** in $CDCl_3$ solution (0.1 M). (b) Solvent-corrected Raman and ROA spectra recorded at 295 K of (+)-**2** and (−)-**2** in $CDCl_3$ solution (0.1 M).

flexibility of the cryptophane derivatives. Indeed, their intensity decreases with the presence of *gauche* conformations in the aliphatic linkers, as already reported in the literature.[26] In contrast, the bands at 1344, 1316, 1030, and 996 cm^{-1} depends only on the number of ethylenedioxy and propylenedioxy linkers.

To confirm the absolute configuration of cryptophane-223 and -233, ab initio calculations at the DFT level have been performed for compounds **1** and **2**. The geometries of $CHCl_3$@*PP*-**1** and $CHCl_3$@*PP*-**2** complexes were optimized at the B3PW91/6-31G** level, and harmonic vibrational frequencies were calculated at the same level. Calculations were performed assuming *trans* and *gauche*−*gauche* conformations for the ethylenedioxy and propylenedioxy linkers, respectively. The comparison of the experimental and calculated VCD spectra of $CHCl_3$@*PP*-**1** and $CHCl_3$@*PP*-**2** complexes are reported in Figure 5, parts a and b, respectively. The VCD spectra calculated for the *PP* configuration reproduce the sign of most of the bands observed in the experimental VCD spectra for the (+)-enantiomers, confirming the absolute configuration (+)-*PP* of cryptophane-223 and -233, as already reported for *anti*-cryptophane derivatives.[21]

Raman and ROA Spectroscopy. Finally, experimental Raman and Raman optical activity (ROA) spectra obtained for 0.1 M chloroform solutions of cryptophanes **1** and **2** are shown in Supporting Information (Figures S11a and S11b, respectively). The Raman spectra of compounds **1** and **2** reveal the difficulty to perform experiments at moderate concentration (0.1 M) since the intensities of the cryptophane peaks, visible essentially in the 1700−1000 cm^{-1} spectral range, are very low with respect to those of the deuterated chloroform solvent at 908, 737, 650, 364, and 260 cm^{-1}. The Raman spectra of the two enantiomers of **1** and **2** exhibit very low fluorescence backgrounds, allowing ROA experiments. ROA spectra of the two enantiomers are nearly perfect mirror images for the two compounds, as expected for enantiopure materials. The ROA spectra presented in Figure 6, parts a and b in the 1800−700 cm^{-1} spectral range were obtained with a good signal-to-noise ratio, allowing a direct comparison between cryptophane derivatives. The ROA spectra of the two compounds reveal strong similarities (Supporting Information, Figure S12), as already mentioned for ECD and VCD experiments. Thus, the cryptophanes **1** and **2** has not been modified enough to observe significant changes in the ROA spectra.

CONCLUSION

In this article, we report a detailed study of the chiroptical properties of cryptophanes **1**−**2**, possessing linkers of different nature (ethylenedioxy and propylenedioxy) connecting the two CTB units. The chiroptical properties of compounds **1** and **2** (C_2-symmetry), determined by polarimetry, ECD, VCD and ROA, are compared to those of the cryptophane-A (**3**, D_3-symmetry), possessing three ethylenedioxy linkers. The two enantiomers of cryptophanes **1**−**2** have been successfully separated by HPLC using chiral stationary phases. A thorough investigation of the chiroptical properties of **1** and **2** reveals that the results obtained for the two compounds are more or less different, depending on the chiroptical techniques used. For

DOI: 10.1021/acs.jpcb.5b04539
J. Phys. Chem. B 2015, 119, 8631−8639

example, the optical rotation values of cryptophanes **1** and **2** are found strongly dependent on the nature of the linkers and large differences are observed between compounds **1**−**2** and cryptophane-A. These values decrease with the number of propylenedioxy linker connecting the two CTB units. On the other hand, relatively small spectral differences have been observed in the ECD spectra of **1**−**2**. TDDFT calculations of the ECD spectra of the $CHCl_3$@*PP*-**1** and $CHCl_3$@*PP*-**2** complexes, performed for a single conformation of the linkers, reproduce fairly well the experimental spectra. VCD spectroscopy shows slight spectral differences for the two $CHCl_3$@*PP*-**1** and $CHCl_3$@*PP*-**2** complexes. DFT calculations of the VCD spectra reproduce well these differences and allow the attribution of the (+)-*PP* absolute configuration for both cryptophanes-223 and -233 in chloroform solution. ROA results lead to similar conclusions. This absolute configuration is in perfect agreement with the configuration determined from the X-ray structures of the two enantiomers of **1** and **2**.

■ ASSOCIATED CONTENT

Supporting Information

Chromatograms of the collected enantiomers of **1** and **2** after preparative separation on Chiralpak IA, view of the crystal packing of **1** and **2**, UV−vis and IR spectra of **1** and **2**, ECD, VCD, and ROA spectra of the two enantiomers of **1** and **2** in chloroform solutions, and ECD spectra of $CHCl_3$@*PP*-**1** and $CHCl_3$@*PP*-**2** complexes calculated by TDDFT. The Supporting Information is available free of charge on the ACS Publications website at DOI: 10.1021/acs.jpcb.5b04539.

■ AUTHOR INFORMATION

Corresponding Authors

*(T.Br.) E-mail: thierry.brotin@ens-lyon.fr.

*(T.Bu.) E-mail: t.buffeteau@ism.u-bordeaux1.fr. Telephone: (33) 5 40 00 63 65.

Author Contributions

The manuscript was written through contributions of all authors. All authors have given approval to the final version of the manuscript.

Notes

The authors declare no competing financial interest.

■ ACKNOWLEDGMENTS

Support from the French Ministry of Research (Project ANR-12-BSV5-0003) is acknowledged. The authors are indebted to the CNRS (Chemistry Department) and to Région Aquitaine for financial support in VCD and ROA equipment. They also acknowledge computational facilities provided by the MCIA (Mésocentre de Calcul Intensif Aquitain) of the Université de Bordeaux and of the Université de Pau et des Pays de l'Adour, financed by the "Conseil Régional d'Aquitaine" and the French Ministry of Research and Technology.

■ REFERENCES

(1) Collet, A. Cyclotriveratrylenes and Cryptophanes. *Tetrahedron* **1987**, *43*, 5725−5759.

(2) Brotin, T.; Dutasta, J.-P. Cryptophanes and Their Complexes: Present and Future. *Chem. Rev.* **2009**, *109*, 88−130.

(3) Spence, M. M.; Ruiz, E. J.; Rubin, S. M.; Lowery, T. J.; Winssinger, N.; Schultz, P. G.; Wemmer, D. E.; Pines, A. Development of a Functionalized Xenon Biosensor. *J. Am. Chem. Soc.* **2004**, *126*, 15287−15294.

(4) Huber, G.; Brotin, T.; Dubois, L.; Desvaux, H.; Dutasta, J.-P.; Berthault, P. Water Soluble Cryptophanes Showing Unprecedented Affinity for Xenon: Candidates as NMR-Based Biosensors. *J. Am. Chem. Soc.* **2006**, *128*, 6239−6246.

(5) Fogarty, H. A.; Berthault, P.; Brotin, T.; Huber, G.; Desvaux, H.; Dutasta, J.-P. A Cryptophane Core Optimized for Xenon Encapsulation. *J. Am. Chem. Soc.* **2007**, *129*, 10332−10333.

(6) Hill, P. A.; Wei, Q.; Troxler, T.; Dmochowski, I. J. Substituent Effects on Xenon Binding Affinity and Solution Behavior of Water-Soluble Cryptophanes. *J. Am. Chem. Soc.* **2009**, *131*, 3069−3077.

(7) Berthault, P.; Desvaux, H.; Wendlinger, T.; Gyejacquot, M.; Stopin, A.; Brotin, T.; Dutasta, J.-P.; Boulard, Y. Effect of pH and Counterions on the encapsulation Properties of Xenon in Water-Soluble Cryptophanes. *Chem. - Eur. J.* **2010**, *16*, 12941−12946.

(8) Fairchild, R. M.; Joseph, A. I.; Holman, K. T.; Fogarty, H. A.; Brotin, T.; Dutasta, J.-P.; Boutin, C.; Huber, G.; Berthault, P. A Water-Soluble Xe@cryptophane-111 Complex Exhibits Very High Thermodynamic Stability and a Peculiar ^{129}Xe NMR Chemical Shift. *J. Am. Chem. Soc.* **2010**, *132*, 15505−15507.

(9) Seward, G. K.; Bai, Y.; Khan, N. S.; Dmochowski, I. J. Cell-Compatible, Integrin-Targeted Cryptophane ^{129}Xe NMR Biosensors. *Chem. Sci.* **2011**, *2*, 1103−1110.

(10) Kotera, N.; Tassali, N.; Léonce, E.; Boutin, C.; Berthault, P.; Brotin, T.; Dutasta, J.-P.; Delacour, L.; Traoré, T.; Buisson, D. A.; et al. Sensitive Zinc-Activated ^{129}Xe MRI Probe. *Angew. Chem., Int. Ed.* **2012**, *51*, 4100−4103.

(11) Sloniec, J.; Schnurr, M.; Witte, C.; Resch-Genger, U.; Schröder, L.; Hennig, A. Biomembrane Interactions of Functionalized Cryptophane-A: Combined Fluorescence and 129Xe NMR Studies of a Bimodal Contrast Agent. *Chem. - Eur. J.* **2013**, *19*, 3110−3118.

(12) Delacour, L.; Kotera, N.; Traoré, T.; Garcia-Argote, S.; Puente, C.; Leteurtre, F.; Gravel, E.; Tassali, N.; Boutin, C.; Léonce, E.; et al. Clickable" Hydrosoluble PEGylated Cryptophane as a Universal Platform for ^{129}Xe Magnetic Resonance Imaging Biosensor. *Chem. - Eur. J.* **2013**, *19*, 6089−6093.

(13) Cavagnat, D.; Buffeteau, T.; Brotin, T. Synthesis and Chiroptical Properties of Cryptophanes Having C_1-Symmetry. *J. Org. Chem.* **2008**, *73*, 66−75.

(14) Traoré, T.; Delacour, L.; Garcia-Argote, S.; Berthault, P.; Cintrat, J.-C.; Rousseau, B. Scalable Synthesis of Cryptophane-1.1.1 and its Functionalization. *Org. Lett.* **2010**, *12*, 960−962.

(15) Taratula, O.; Aru Hill, P.; Bai, Y.; Khan, N. S.; Dmochowski, I. J. Shorter Synthesis of Trifunctionalized Cryptophane-A Derivatives. *Org. Lett.* **2011**, *13*, 1414−1417.

(16) Brotin, T.; Cavagnat, D.; Jeanneau, E.; Buffeteau, T. Synthesis of Highly Substituted Cryptophane Derivatives. *J. Org. Chem.* **2013**, *78*, 6143−6153.

(17) Tyagi, R.; Witte, C.; Haag, R.; Schröder, L. Dendronized Cryptophanes as Water-Soluble Xenon Hosts for ^{129}Xe Magnetic Resonance Imaging. *Org. Lett.* **2014**, *16*, 4436−4439.

(18) IUPAC. Tentative Rules for the Nomenclature of Organic Chemistry. Section E. Fundamental Stereochemistry. *J. Org. Chem.* **1970**, *35*, 2849−2867.

(19) Collet, A.; Gabard, G.; Jacques, J.; Césario, M.; Guilhem, J.; Pascard, C. Synthesis and Absolute Configuration of Chiral (C_3) Cyclotriveratrylene Derivatives. Crystal Structure of (*M*)-(−)2,7,12-Triethoxy-3,8,13-tris-[(*R*)-1-methoxycarbonylethoxy]-10,15-dihydro-5*H*-tribenzo[*a*,*d*,*g*]-cyclononene. *J. Chem. Soc., Perkin Trans. 1* **1981**, 1630−1638.

(20) Canceill, J.; Lacombe, L.; Collet, A. Analytical Optical Resolution of Bromochlorofluoromethane by Enantioselective Inclusion into a Tailor-Made "Cryptophane" and Determination of Its Maximum Rotation. *J. Am. Chem. Soc.* **1985**, *107*, 6993−6996.

(21) Brotin, T.; Vanthuyne, N.; Cavagnat, D.; Ducasse, L.; Buffeteau, T. Chiroptical Properties of Nona- and Dodecamethoxy Cryptophanes. *J. Org. Chem.* **2014**, *79*, 6028−6036.

(22) Canceill, J.; Collet, A.; Gottarelli, G.; Palmieri, P. Synthesis and Exciton Optical Activity of D_3-Cryptophanes. *J. Am. Chem. Soc.* **1987**, *109*, 6454−6464.

DOI: 10.1021/acs.jpcb.5b04539
J. Phys. Chem. B 2015, 119, 8631−8639

(23) Zhong, Z.; Ikeda, A.; Shinkai, S.; Sakamoto, S.; Yamaguchi, K. Creation of Novel Chiral Cryptophanes by a Self Assembling Method Utilizing a Pyridil-Pd(II) Interaction. *Org. Lett.* **2001**, *3*, 1085−1087.
(24) Brotin, T.; Barbe, R.; Darzac, M.; Dutasta, J. P. Novel Synthetic Approach for Optical Resolution of Cryptophanol-A: A Direct Access to Chiral Cryptophanes and Their Chiroptical Properties. *Chem. - Eur. J.* **2003**, *9*, 5784−5792.
(25) Brotin, T.; Cavagnat, D.; Dutasta, J.-P.; Buffeteau, T. Vibrational Circular Dichroism Study of Optically Pure Cryptophane-A. *J. Am. Chem. Soc.* **2006**, *128*, 5533−5540.
(26) Brotin, T.; Cavagnat, D.; Buffeteau, T. Conformational Changes in Cryptophane Having C_1-Symmetry Studied by Vibrational Circular Dichroism. *J. Phys. Chem. A* **2008**, *112*, 8464−8470.
(27) Bouchet, A.; Brotin, T.; Cavagnat, D.; Buffeteau, T. Induced Chiroptical Changes of a Water-Soluble Cryptophane by Encapsulation of Guest Molecules and Counterion Effects. *Chem. - Eur. J.* **2010**, *16*, 4507−4518.
(28) Bouchet, A.; Brotin, T.; Linares, M.; Agren, H.; Cavagnat, D.; Buffeteau, T. Conformational Effects Induced by Guest Encapsulation in an Enantiopure Water-Soluble Cryptophane. *J. Org. Chem.* **2011**, *76*, 1372−1383.
(29) Bouchet, A.; Brotin, T.; Linares, M.; Agren, H.; Cavagnat, D.; Buffeteau, T. Enantioselective Complexation of Chiral Propylene Oxide by an Enantiopure Water-Soluble Cryptophane. *J. Org. Chem.* **2011**, *76*, 4178−4181.
(30) Bouchet, A.; Brotin, T.; Linares, M.; Cavagnat, D.; Buffeteau, T. Influence of the Chemical Structure of Water-Soluble Cryptophanes on Their Overall Chiroptical and Binding Properties. *J. Org. Chem.* **2011**, *76*, 7816−7825.
(31) Brotin, T.; Montserret, R.; Bouchet, A.; Cavagnat, D.; Linares, M.; Buffeteau, T. High Affinity of Water-Soluble Cryptophanes for Cesium Cations. *J. Org. Chem.* **2012**, *77*, 1198−1201.
(32) Brotin, T.; Cavagnat, D.; Berthault, P.; Montserret, R.; Buffeteau, T. Water-Soluble Molecular Capsule for the Complexation of Cesium and Thallium Cations. *J. Phys. Chem. B* **2012**, *116*, 10905−10914.
(33) Taratula, O.; Kim, M. P.; Bai, Y.; Philbin, J. P.; Riggle, B. A.; Haase, D. N.; Dmochowski, I. J. Synthesis of Enantiopure Trisubstituted Cryptophane-A Derivatives. *Org. Lett.* **2012**, *14*, 3580−3583.
(34) Brotin, T.; Goncalves, S.; Berthault, P.; Cavagnat, D.; Buffeteau, T. Influence of the Cavity Size of Water-Soluble Cryptophanes on Their Binding Properties for Cesium and Thallium Cations. *J. Phys. Chem. B* **2013**, *117*, 12593−12601.
(35) Wang, T.; Zhang, Yu-Fei.; Hou, Q.-Q.; Xu, W.-R.; Cao, X.-P.; Chow, H.-F.; Kuck, D. C_3-Symmetrical Tribenzotriquinacene Derivatives: Optical Resolution Through Cryptophane Synthesis and Supramolecular Self-Assembly into Nanotubes. *J. Org. Chem.* **2013**, *78*, 1062−1069.
(36) Daugey, N.; Brotin, T.; Vanthuyne, N.; Cavagnat, D.; Buffeteau, T. Raman Optical Activity of Enantiopure Cryptophanes. *J. Phys. Chem. B* **2014**, *118*, 5211−5217.
(37) Brotin, T.; Dutasta, J.-P. Xe@cryptophane Complexes with C_2 Symmetry: Synthesis and Investigations by ^{129}Xe NMR of the Consequences of the Size of the Host Cavity for Xenon Encapsulation. *Eur. J. Org. Chem.* **2003**, *2003*, 973−984.
(38) CrysAlisPro, Agilent Technologies, Version 1.171.34.49 (release 20−01−2011 CrysAlis171.NET) (compiled Jan 20 2011,15:58:25).
(39) Clark, R. C.; Reid, J. S. The Analytical Calculation of Absorption in Multifaceted Crystals. *Acta Crystallogr.* **1995**, *A51*, 887−897.
(40) Altomare, A.; Burla, M. C.; Camalli, M.; Cascarano, G. L.; Giacovazzo, C.; Guagliardi, A.; Grazia, A.; Moliterni, G.; Polidori, G.; Spagna, R. *SIR97*: A New Tool for Crystal Structure Determination and Refinement. *J. Appl. Cryst.* **1999**, *32*, 115−119.
(41) Betteridge, P. W.; Carruthers, J. R.; Cooper, R. I.; Prout, K.; Watkin, D. J. *CRYSTALS* version 12: Software for Guided Crystal Structure Analysis. *J. Appl. Crystallogr.* **2003**, *36*, 1487.
(42) Van Der Sluis, P.; Spek, A. L. BYPASS: An Effective Method for the Refinement of Crystal Structures Containing Disordered Solvent Regions. *Acta Cryst. A* **1990**, *46*, 194−201.
(43) Buffeteau, T.; Lagugné-Labarthet, F.; Sourrisseau, C. Vibrational Circular Dichroism in General Anisotropic Thin Solid Films: Measurement and Theoretical Approach. *Appl. Spectrosc.* **2005**, *59*, 732−745.
(44) Nafie, L. A.; Vidrine, D. W. In *Fourier Transform Infrared Spectroscopy*, Ferraro, J. R., Basile, L. J., Eds.; Academic Press: New York, 1982; Vol. 3, pp 83−123.
(45) Hug, W.; Hangartner, G. A Novel High-throughput Raman Spectrometer for Polarization Difference Measurements. *J. Raman Spectrosc.* **1999**, *30*, 841−852.
(46) Hug, W. Virtual Enantiomers as the Solution of Optical Acitivity's Deterministic Offset Problem. *Appl. Spectrosc.* **2003**, *57*, 1−13.
(47) Frisch, M. J.; Trucks, G. W.; Schlegel, H. B.; Scuseria, G. E.; Robb, M. A.; Cheeseman, J. R.; Scalmani, G.; Barone, V.; Mennucci, B.; Petersson, G. A. et al. *Gaussian 09*, revision A.1, Gaussian Inc.: Wallingford CT, 2009.
(48) Perdew, J. P.; Wang, Y. Accurate and Simple Analytic Representation of the Electron-Gas Correlation Energy. *Phys. Rev. B* **1992**, *45*, 13244−13249.
(49) Ditchfield, R.; Hehre, W. J.; Pople, J. A. Self-Consistent Molecular-Orbital Methods. IX. An Extended Gaussian-Type Basis for Molecular-Orbital Studies of Organic Molecules. *J. Chem. Phys.* **1971**, *54*, 724−728.
(50) Lynch, B. J.; Fast, P. L.; Harris, M.; Truhlar, D. G. Adiabatic Connection for Kinetics. *J. Phys. Chem. A* **2000**, *104*, 4811−4815.
(51) Tomasi, J.; Persico, M. Molecular Interactions in Solution: An Overview of Methods Based on Continuous Distributions of the Solvent. *Chem. Rev.* **1994**, *94*, 2027−2094.
(52) Tomasi, J.; Mennucci, B.; Cammi, R. Quantum Mechanical Continuum Solvation Models. *Chem. Rev.* **2005**, *105*, 2999−3094.
(53) The ethylenedioxy linker may adopt three conformations: One *trans* (T) conformation with the O−C−C−O dihedral angles of ± 180° and two *gauche* (G_+ and G_-) conformations with the O−C−C−O dihedral angles of +60° and −60°, respectively. The propylenedioxy linker may adopt nine conformations: TT, TG_+, TG_-, G_+T, G_+G_+, G_+G_-, G_-T, G_-G_+, and G_-G_-.
(54) Perraud, O.; Raytchev, P. D.; Martinez, A.; Dutasta, J.-P. Resolution and Absolute Configuration Assignment of a Chiral Hemicryptophane Molecular Cage. *Chirality* **2010**, *22*, 885−888.

DOI: 10.1021/acs.jpcb.5b04539
J. Phys. Chem. B 2015, 119, 8631−8639